INFRARED PROPERTIES OF SOLID TITANIUM OXIDES: EXPLORING POTENTIAL PRIMARY DUST CONDENSATES

TH. POSCH AND F. KERSCHBAUM

Institut für Astronomie, Türkenschanzstraße 17, A-1180 Wien, Austria; posch@astro.univie.ac.at

D. FABIAN, H. MUTSCHKE AND J. DORSCHNER

Astrophysikalisches Institut und Universitätssternwarte, Schillergäßchen 2-3, D-07745 Jena, Germany

A. TAMANAI

Zentrum für Astronomie und Astrophysik, TU Berlin, Hardenbergstraße 36, D-10623 Berlin, Germany

AND

TH. HENNING

Max-Planck-Institut für Astronomie (MPIA), Königstuhl 17, D-69117 Heidelberg, Germany

ABSTRACT

We present optical constants and opacities of solid TiO_2, Ti_2O_3, magnesium and calcium titanates, largely based on laboratory measurements. These dust species deserve interest as potential primary condensates in oxygen-rich dusty environments. Of the three known solid TiO_2 phases, only one (rutile) has been extensively studied so far with respect to its mid-IR optical properties. We compare these with our measurements of the optical constants of anatase, brookite, and $CaTiO_3$. Furthermore, for several Mg-Ti-oxides, powder transmission spectra are shown. While all known TiO_2 modifications have their strongest bands between 13 and 13.5 μm (for spherical particles), $CaTiO_3$, $MgTiO_3$, and other Mg titanates have principal maxima of their absorption coefficients between 14 and 19 μm. This makes a spectroscopic identification of circumstellar Ti oxide particles rather difficult, because both the 13 and the 14–19 μm region are crowded with other features in the spectra of oxygen-rich circumstellar shells.

Subject headings: circumstellar matter — methods: laboratory — molecular data — solar system: formation — stars: AGB and post-AGB — stars: mass loss

1. INTRODUCTION

Since the classical reviews by Barshay & Lewis (1976) and Salpeter (1977), titanium oxides are considered—together with calcium and aluminium oxides—as candidates for the very first condensates in oxygen-rich environments (both in the primitive solar nebula and in chemically comparable circumstellar shells.) More recent works on condensation of dust in a gas of solar composition, such as Ebel & Grossman (2000), confirm that Ti oxides (especially $CaTiO_3$) are among the highest temperature condensates. Of course, titanium is rather rare according to its mean cosmic elemental abundance, which is 2.5 orders of magnitude smaller than that of silicon and magnesium and about 1.5 orders of magnitude smaller than that of aluminium and calcium. However, with respect to dust formation in circumstellar shells, it is important to note that the TiO *molecule* is rather prominent in the atmospheres of M and S stars, a fact that is partly due to the high bond energy of TiO (6.9 eV). In the interstellar gas, on the other hand, Ti and Ca are heavily depleted, indicating that these atoms have indeed been consumed by dust formation processes.

Jeong et al. (Jeong, Winters, & Sedlmayr 1999; Jeong et al. 2003) predicted TiO_2 to be the most promising candidate for the primary condensate in oxygen-rich circumstellar shells. They expect this dust species to form at a temperature above 1000 K—corresponding to a distance from the center of the star of only two stellar radii—and to enter into a heterogeneous growth process, resulting in grains with an onion-like structure and composed of different oxides. Mainly, the grain cores would contain TiO_2, according to this scenario.

In the atmospheres of brown dwarfs, the occurrence of titanium oxides is also very likely, both because of the observed depletion of heavy elements in the gas phase and in view of predicted condensation sequences. Helling et al. (2001) examined the nucleation efficiency of several molecules in brown dwarf atmospheres. They came to the conclusion that TiO_2 and $CaTiO_3$ are likely to be among the first nuclei in such environments, even though other substances may be more important as growth species. Burrows & Sharp (1999) showed that it depends on the brown dwarf's effective temperature, which titanium oxide is the first condensate to form. For effective temperatures above 2000 K, it is $CaTiO_3$, whereas for lower temperatures, it is Ti_3O_5.

There are only three more or less direct indications for the formation of titanium compounds in circumstellar shells. First, a presolar meteoritic TiO_2 grain has been tentatively identified (Nittler 2003). The grain was in a mixed residue of the Bishunpur, Krymka, Semarkona, and Tieschitz unequilibrated ordinary chondrites (L. R. Nittler 2003, private communication) Second, the 20.1 μm feature observed in the spectra of post-AGB stars has been attributed to titanium carbide clusters by von Helden et al. (2000). (A more recent detailed study of the same feature by Hony et al. (2003), however, showed that this identification is questionable.) Third, a number of TiC particles have also been found as cores of presolar graphite spherules in the Murchison meteorite (see Bernatowicz et al. 1996; the authors underline

that the TiC crystals can have formed in AGB star atmospheres only in regions with locally increased densities—see also Chigai, Yamamoto, & Kozasa 1999).

Apart from this, there is no observational evidence for the occurrence of solid titanium compounds as stardust minerals up to now. It is probable, though, that this situation will change during the coming years when high-resolution spectroscopy of circumstellar shells become feasible, e.g., with the infrared spectrographs of the Very Large Telescope (VLT). Work of this kind can be prepared more effectively based on information on the optical properties of titanates, which is crucial for identifying previously unknown dust features.

The present article is meant as a contribution to this goal. It is structured as follows. In § 2, we discuss the optical properties of the TiO_2 modifications rutile, anatase, and brookite as well as those of Ti_2O_3. In § 3, opacities of calcium and magnesium titanates are presented. In the last section (§ 4), the astrophysical implications of our work are briefly illustrated. In a forthcoming paper, results of condensation experiments with titanium (and other) oxides will be compared with the results of this work.

2. SOLID TITANIUM OXIDES OF Ti_xO_y COMPOSITION

Up to date, four naturally occurring modifications of solid titanium dioxide are known: rutile, anatase, $TiO_2(B)$, and brookite. On Earth, the tetragonal *rutile* is the most abundant of them. At least three further TiO_2 polymorphs can be synthetically produced (see Banfield & Veblen (1992) for an overview of the properties both of the natural and of the synthetic polymorphs). Recently, an ultradense TiO_2 polymorph has been discovered in shocked gneisses of the Ries crater (El Goresy et al. 2001). However, those modifications of TiO_2 which are only formed under high pressures can of course not be expected to occur in circumstellar shells.

Rutile's optical constants are sufficiently well known in the spectral range between 11 and 36 μm (see, e.g., Ribarsky 1985). On the basis of these optical data, absorption efficiencies both for spherical and for ellipsoidal sub-micron sized rutile particles have been calculated by Posch et al. (1999). In the same paper, calculations of the emissivities of core-mantle particles containing rutile have been presented. In view of this, we will restrict ourselves to giving some additional information on rutile in § 2.1 and to use its reflectance as well as small particle spectra as a reference for the other titanium dioxide spectra.

Apart from rutile, the following other TiO_2 polymorphs occur naturally: *anatase*, which also belongs to the tetragonal crystal class, the monoclinic *$TiO_2(B)$*, and the rhombic *brookite*. Both anatase and brookite have also been identified in meteorites, but there is no information concerning their solar system or presolar origin (Ulyanov 1998). Since there are, as far as we know, no predictions concerning the question in which structure solid TiO_2 might form in circumstellar envelopes, we consider it important to also discuss the IR optical properties of brookite and anatase (see §§ 2.2 and 2.3).[1]

2.1. *Rutile*

Rutile is a highly refractory material. Its melting point at atmospheric pressure amounts to 2116 K (Holleman &

[1] See http://www.astro.uni-jena.de.

Wiberg 1995). Its basic structural unit is a TiO_6 octahedron, which is constituted by a Ti^{4+} ion coordinated by six O^{2-} ions. Each such TiO_6 octahedron is slightly distorted and forms a chain of edge sharing octahedra with its neighbors.

As already mentioned, the IR optical properties of rutile have been studied extensively. Therefore, we will only summarize an astrophysically relevant peculiarity here, namely the strong temperature dependence of rutile's dielectric function. Gervais & Piriou (1974b) have examined this dependence in the temperature range 295–1475 K. They showed that the maxima of the imaginary part of the dielectric function become decreasingly prominent with increasing temperature. Technically speaking, the damping constants γ_i of the resonance modes increase by factors between 3.5 and 4.6 in the above mentioned temperature interval. (This behavior is called hardening of the modes with increasing temperature.) One of the resonance modes, expected to produce a 27.5 μm emissivity maximum, will even vanish for dust temperatures above 1000 K.

Clearly, this may have significant consequences for the possibility of detecting TiO_2 dust particles by means of IR spectroscopy. First of all, we expect to see only *two* emission bands arising from hot, spherical rutile particles, namely at 13.4 and at 23 μm—whereas on the basis of the room temperature optical constants given by Ribarsky (1985), one would expect a characteristic pattern of *three* bands, the third one being positioned at 27.5 μm. Second, the remaining two spectral features of the hot dust will be, due to the hardening of the modes, *much less prominent* than in the case of cooler dust.

2.2. *Anatase*

Anatase is the low-temperature and low-pressure modification of tetragonal titanium dioxide. It also consists of chains of TiO_6 octahedra. Each of these octahedra is distorted, even more than in the case of rutile, such that four O-Ti-O angles deviate from 90°. The Ti-Ti distances are smaller in anatase than in rutile, while the Ti-O distances are greater. The overall density of anatase is smaller than that of rutile by almost 10% (Linsebigler, Lu, & Yates 1995).

By thermal annealing, anatase is transformed into rutile (Won et al. 2001). The transformation to rutile takes place at temperatures above 1200 K. By measuring its reflectance spectrum on natural crystals, we studied this structural transformation, in addition to aiming at a derivation of the optical constants of (unannealed) anatase.

Figure 1 shows the polarized reflectance spectrum of an unannealed anatase crystal from Diamantina, Brazil (with face diameters of 0.4 cm), and, for comparison, the corresponding room temperature reflectance of rutile (measured on a 0.5×1 cm^2 polished crystal from Modriach, Austria). These two pairs of spectra represent the extremes of the possible IR spectra of tetragonal TiO_2 in the sense that rutile can be understood as "fully annealed" anatase.

The spectroscopic effects of "partial annealing" of another anatase crystal (from Hardangervidda, Norway) are shown in Figure 2. In this figure, we present exclusively unpolarized spectra, since these are sufficient for studying the structural transition. What we compare here with the reflectance spectrum of the natural crystal is (*a*) the spectrum of a sample that has been exposed to a temperature of 1273 K for 10 minutes and (*b*) the spectrum of the same
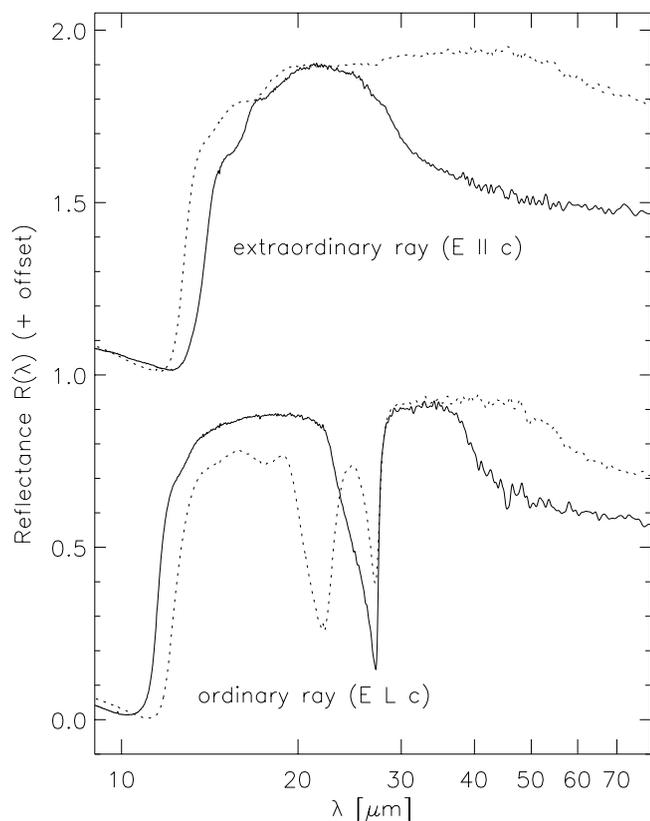
FIG. 1.—Polarized reflectance spectra of anatase (*solid lines*) compared to those of rutile, also shown (*dotted lines*). The spectra for $E \parallel c$ were shifted vertically by an amount of 1.0.

sample after 10 minutes of annealing at a temperature of 1323 K. Whereas the first spectrum closely resembles that of the natural crystal, the second shows the reflectance minimum at 22.1 μm, which is characteristic of rutile.

We may infer from these results that anatase can only be present in environments where it is *not* exposed to temperatures significantly higher than 1300 K. According to Gail & Sedlmayr (1998), the stability limit for the formation of solid TiO_2 exceeds 1300 K only at pressures above 5×10^{-3} dyn
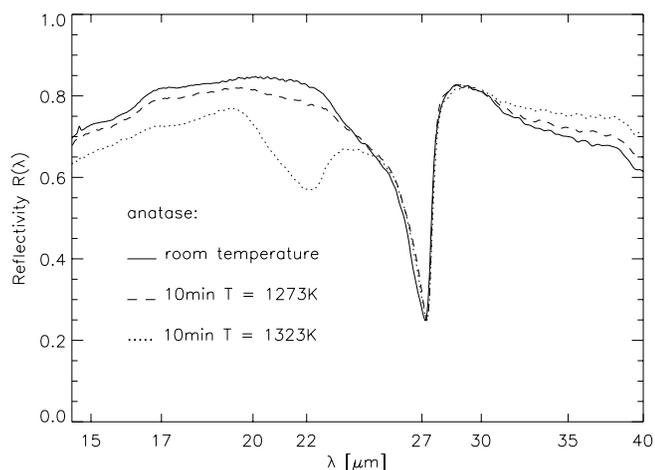
cm^{-2}; in other words, at lower pressures, the formation of solid TiO_2 will take place at temperatures *below* the anatase-rutile conversion temperature. Under these conditions (which are well within the range of parameters expected to characterize the condensation zones of circumstellar shells), anatase grains can form, whereas at higher temperatures, we can only expect the formation of rutile grains.

Note that both rutile and anatase (but especially the latter) have very peculiar reflectances. The large, plateau-like maximum of $R(\lambda)$, which extends from 13 to 20 μm for the ordinary ray in anatase, indicates very strong lattice resonances and, correspondingly, large values of the optical constants.

Because of this peculiarity, the classical Lorentz oscillator fit is inadequate for deriving the optical constants of the two tetragonal TiO_2 modifications. As was first shown by Gervais & Piriou (1974a), another approach has to be chosen for rutile, and the same holds for anatase. The dielectric function is to be written in a factorized form:

$$\epsilon(\omega) = \epsilon_\infty \prod_j \frac{\Omega_{j,\mathrm{LO}}^2 - \omega^2 + i\gamma_{j,\mathrm{LO}}\omega}{\Omega_{j,\mathrm{TO}}^2 - \omega^2 - i\gamma_{j,\mathrm{TO}}\omega} , \qquad (1)$$

where $\Omega_{j,\mathrm{LO/TO}}$ is the respective oscillator strength for the longitudinal/transverse (LO/TO) optical mode and $\gamma_{j,\mathrm{LO/TO}}$ is the LO/TO damping constant. Note that this formula involves four (instead of three) adjustable parameters for each phonon mode, which is essentially a consequence of the discrimination between $\gamma_{j,\mathrm{LO}}$ and $\gamma_{j,\mathrm{TO}}$—whereas within classical dispersion theory, there is only one damping constant for each oscillator. The latter model assumption is appropriate only as long as the difference between $\Omega_{j,\mathrm{LO}}$ and $\Omega_{j,\mathrm{TO}}$ is small compared to their absolute values.

Using equation (1), Gonzalez & Zallen (1997) have calculated the mid-IR dielectric function of anatase. However, their set of parameters leads to negative values of the imaginary part of $\epsilon(\omega)$ for large values of ω. Therefore, we had to derive the optical constants of anatase independently of Gonzalez & Zallen's work. Our oscillator frequencies and damping constants are listed in Table 1; the resulting $n(\lambda)$- and $k(\lambda)$-functions are shown in Figure 3.

FIG. 2.—Unpolarized reflectance spectra of an anatase crystal before annealing and for two different annealing temperatures (1273 and 1323 K). For the higher annealing temperatures, an additional reflectance minimum characteristic of the rutile structure appears.

TABLE 1

OUR SET OF OSCILLATOR PARAMETERS ENTERING INTO THE DIELECTRIC FUNCTION OF ANATASE

j	$\Omega_{j,\mathrm{TO}}$	$\gamma_{j,\mathrm{TO}}$	$\Omega_{j,\mathrm{LO}}$	$\gamma_{j,\mathrm{LO}}$
1$_{\mathrm{OR}}$	0.0	0.0	0.0	0.0
2$_{\mathrm{OR}}$	268.1	15.0	367.8	15.0
3$_{\mathrm{OR}}$	0.0	0.0	0.0	0.0
4$_{\mathrm{OR}}$	795.1	100.0	790.3	100.0
5$_{\mathrm{OR}}$	440.0	31.6901	872.8	31.69
1$_{\mathrm{ER}}$	563.3	24.6562	562.6	23.9947
2$_{\mathrm{ER}}$	0.0	0.0	0.0	0.0
3$_{\mathrm{ER}}$	616.1	31.5790	615.4	30.1073
4$_{\mathrm{ER}}$	634.7	40.6265	633.1	39.8176
5$_{\mathrm{ER}}$	354.5	46.0952	746.6	62.9184

NOTES.—The upper part of the table contains the values for the ordinary ray (OR), and the lower part lists the values for the extraordinary ray (ER). For the dielectric background, we adopted the value $\epsilon_\infty = 5.8$ in the case of the ordinary ray and $\epsilon_\infty = 5.4$ in the case of the extraordinary ray. The Ω_j- and γ_j-values are given in units of cm^{-1}.
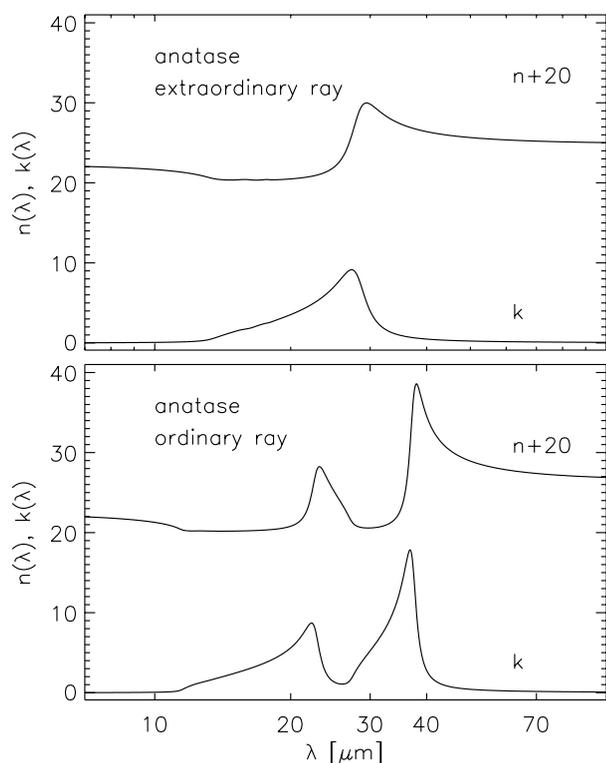
FIG. 3.—Optical constants of (nonannealed) anatase derived from the polarized reflectance spectra shown in Fig. 1.

Based on these optical constants, we calculated the absorption efficiency $C_{abs}(\lambda)$ of small, spherical anatase particles and compared them with the $C_{abs}(\lambda)$-values for (non-elongated) rutile grains. In both cases, the appropriate mixing rule for ordinary and extraordinary rays has been applied. Figure 4 shows the result. There is a rough agreement between rutile's and anatase's absorption efficiency in the 13 and 27.5 μm region, even though the 13 μm emissivity maximum of anatase is shifted to a shorter wavelength by 0.4 μm compared to rutile and the bandwidth is smaller by about 30%. The most conspicuous difference, however, between $C_{abs}(\lambda)$ of anatase and that of rutile is the existence
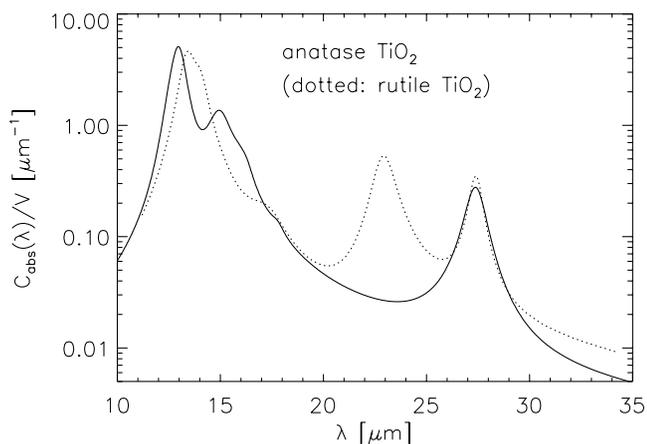
of an additional feature at 15 μm and, on the other hand, the complete lack of a feature at 23 μm for anatase particles.

According to our results, anatase is certainly among the potential carriers of the 13 μm feature. As long as the secondary features of anatase particles at 15 and 27.5 μm remain unobserved, there are no sufficient reasons to argue that this particular dust species is the 13 μm band carrier. However, recent results by Sloan et al. (2003) indicate that there does exist a feature at 28 μm in sources of the 13 μm feature, the strength of which is even correlated with the latter.

2.3. Brookite

Brookite is yet another low-temperature modification of TiO_2. It has an orthorhombic crystal structure, such that it is optically biaxial and has a reduced symmetry compared to rutile and anatase. As far as we are aware, no optical constants of this substance have been derived yet, even though powder transmission spectra of this mineral were published already by Tarte (1963). We performed reflection measurements on a 1×1 cm^2 sample from Virgen (Eastern Tyrol) using a Bruker 113v FTIR spectrometer. The measurements were carried out for three different relative orientations of the electric field vector and the crystal: $E \parallel x$, $E \parallel y$, and $E \parallel z$ (x, y, and z being the three unit vectors representing the three crystallographic axes); see Figure 5 for the respective results.

In contrast to the peculiar cases of rutile and anatase, the optical constants of brookite may be derived by means of classical dispersion theory, i.e., the dielectric functions can

FIG. 4.—Emissivity of anatase in the Rayleigh case. For comparison, the small particle spectrum of rutile is also shown (dotted line). The latter is based on the optical constants published by Ribarsky (1985).
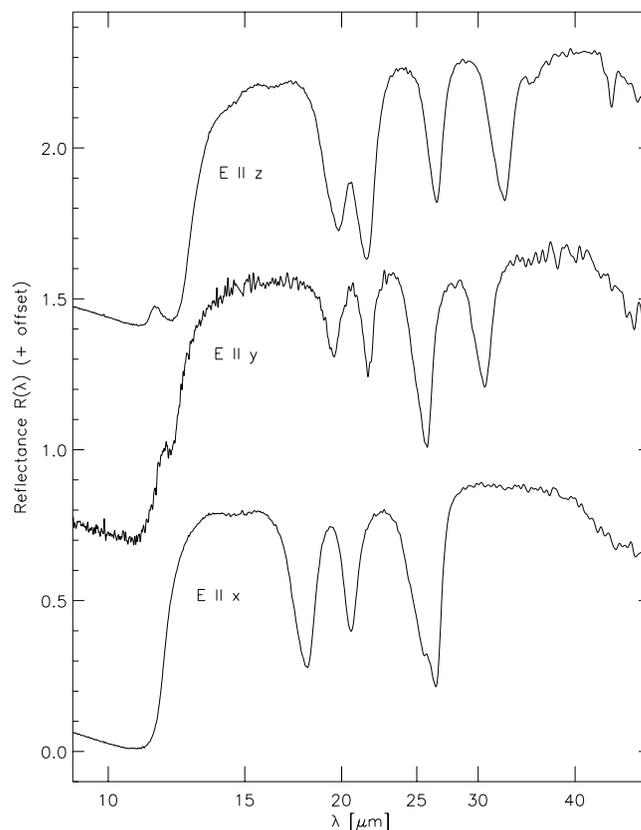
FIG. 5.—Polarized reflectance spectra of brookite (orthorhombic TiO_2). The measurements have been carried out for three different orientations of the electric field vector. The results for $E \parallel y$ and $E \parallel$ were shifted vertically by amounts of 0.6 and 1.2, respectively.
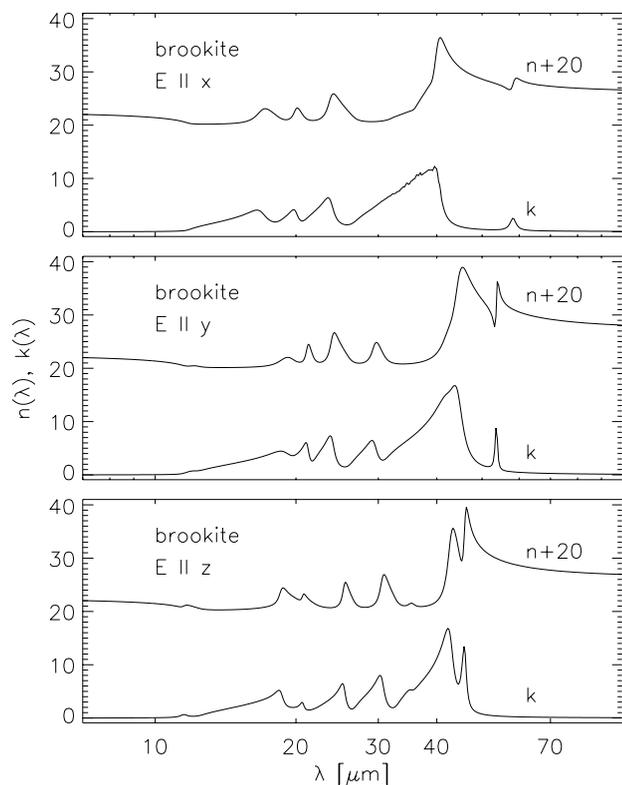
FIG. 6.—IR optical constants of brookite. Note the large values that both n and k reach. The quantity n was shifted vertically by an amount of 20.

FIG. 7.—Emissivity of brookite particles in the Rayleigh case

be expressed in terms of a sum of individual Lorentz oscillators:

$$\epsilon(\omega) = \epsilon_\infty + \sum_j \frac{\Omega_j^2}{\omega_{j,\mathrm{TO}}^2 - \omega^2 - i\gamma_j\omega} , \qquad (2)$$

where Ω_j is the respective oscillator strength, γ_j is the damping constant, and $\omega_{j,\mathrm{TO}}$ is the resonance frequency of the jth oscillator. By combining an oscillator fit according to (2) with a Kramers-Kronig analysis, we derived the optical constants shown in Figure 6 for an electric field vector parallel to the three principal crystallographic axes x, y, and z, respectively.

To derive the effective absorption (and scattering) cross sections of arbitrarily oriented particles, an unweighted mean of the C_{abs}-values for x, y, and z has been calculated. The result is shown in Figure 7. Whereas the profiles of C_{abs} for polarized radiation peak at wavelengths other than 13.5 μm (namely at 13.0, 13.45, and 13.7 μm, respectively), the effective absorption cross section of spherical brookite particles peaks at 13.5 μm—similar as for rutile. Further maxima of C_{abs} are located—again for spherical, submicron sized particles—at 18.5, 21.9, 26.9, 31.1, 33, 44.9, 53.3, and 57.5 μm.

2.4. Ti_2O_3 and Other Solid Ti Oxides

Apart from the three naturally occurring modifications of TiO_2, quite a number of other solid Ti oxides with the general formula Ti_xO_y are known. Among them are Ti_2O_3, Ti_3O_5, and the so-called Magnéli phases Ti_5O_9 and Ti_8O_{15}.

The relevance of these compounds in an astrophysical context is underlined both by the calculations of Jeong et al.

(1999, 2000, 2003) and by the fact that the so-called Magnéli phases are a common component in some interplanetary dust particles (Brearley 1993).

Ti_2O_3 is isostructural to corundum (α-Al_2O_3) and is stable up to very high temperatures, its melting point amounting to 2400 K (after Holleman & Wiberg 1995). Its optical constants have been derived by Lucovsky, Allen, & Sladek (1977). Based on these data, we have calculated absorption efficiencies for the Rayleigh case. The result is shown in Figure 8. The strongest resonance bands are located at 18.6, 25.5, 28.5, and 35.7 μm. Compared to the three modifications of TiO_2 that have been discussed above, the maximum values of the absorption efficiency of Ti_2O_3 are rather small (C_{abs}/V does not exceed 0.6 μm^{-1}, which is only one-tenth of the maximum values for crystalline TiO_2). This fact will strongly hamper the spectroscopic identification of Ti_2O_3 dust.

2.5. Remark on Size and Shape Effects

Until now, we have been considering the absorption efficiencies exclusively of small, spherical Ti_xO_y particles. This restriction can be justified by the assumption that the spherical shape is the most probable case and that titanium oxides, in view of their likely role as condensation nuclei, will not reach large sizes (say, radii of several μm) before mantles
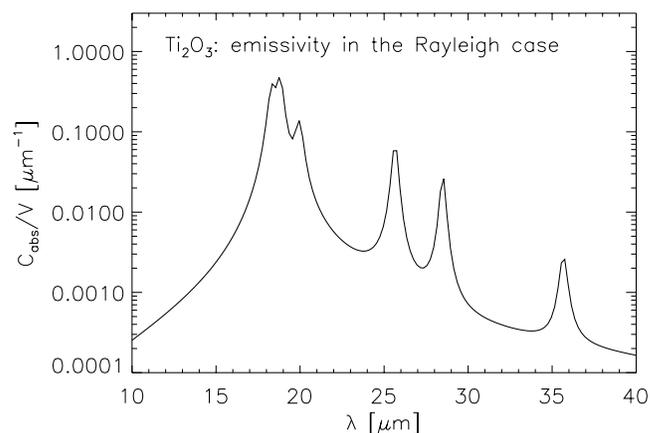
FIG. 8.—Emissivity of small spherical Ti_2O_3 particles

composed of other oxides and silicated grow onto their surfaces.

However, in order to quantify the possible effect of the presence of larger particles, we calculated C_{abs}/V using Mie theory for rutile, anatase, and brookite. The result of these calculations can be briefly summarized as follows: For particle radii up to 1 μm, only a small shift of the peak position of the 13–13.5 μm C_{abs}-maximum of the mentioned TiO$_2$ modifications occurs. If, however, the particle radius reaches 2 μm, there is an unsteady change in the shape of $C_{abs}(\lambda)$. The 13–13.5 μm C_{abs}-maximum does no longer dominate the profile of the absorption efficiency, but decreases in its strength, becoming comparable to the minor C_{abs}-maxima at longer wavelengths. It is evident that such a behavior would make it even more difficult to detect TiO$_2$ particles spectroscopically. But—as mentioned above—it is questionable whether such particles larger than 4 μm in diameter are present in circumstellar shells in significant amounts.

As for the size effects, they are rather strong for TiO$_2$ particles because of their large intrinsic oscillator strengths, corresponding to a large distance (in frequency or wavelength units) between the transverse and the longitudinal optical frequencies. For rutile, e.g., the wavelengths corresponding to the principal TO and LO frequencies differ from each other by about 41 μm or by a factor greater than 4. They amount to $\lambda_1 = 12.03$ μm and $\lambda_2 = 52.91$ μm, implying that for an arbitrary particle shape, the principle maxima of the rutile's absorption efficiency factor are located somewhere in the huge interval between λ_1 and λ_2 (Bohren & Huffman 1983). Of course, this does not mean that for nonspherical rutile particles, the profile of $C_{abs}(\lambda)$ becomes arbitrary. Particular ellipsoidal shapes correspond to well-defined patterns of C_{abs}-maxima. For example, in case of elongated ellipsoids with an axis ratio of 3 : 1, rutile particles can produce something like a 13 μm feature, but a *second*, even more prominent C_{abs}-maximum centered at 16 μm would arise (from rays passing the elongated ellipsoid parallel to its minor axis). Since none of the feature patterns predicted for nonspherical TiO$_2$ particles has been observed so far and since the occurrence of TiO$_2$ particles with axis ratios strongly different from 1 : 1 is unlikely, we do not cover this topic in a more detailed way.

3. Ca-Ti AND Mg-Ti OXIDES

Apart from pure titanium oxides, we also studied the IR optical properties of selected titanates with the general formula $M_x Ti_y O_z$, M denoting one of the metal ions Ca and Mg, which are both more abundant in oxygen-rich environments than titanium itself is. All of the titanates on which we performed measurements are highly refractory, and three of them—CaTiO$_3$, MgTiO$_3$ and MgTi$_2$O$_5$—have been considered as potential primary dust condensates (see, e.g., Gail & Sedlmayr 1998).

Only in the case of CaTiO$_3$ were we able to acquire a sufficiently pure and large single crystal ($\sim$4 $\times$ 4 $\times$ 4 mm^3) to perform reflectance measurements on its surfaces and to derive optical constants from these measurements. As for the Mg titanates, we synthesized polycrystalline samples of them in the laboratory. With these samples, only powder transmission measurements could be performed.

MgTiO$_3$ and MgTi$_2$O$_5$ have been thermally synthesized. Powders of TiO$_2$ and MgCO$_3$ have been mixed in the corresponding stoichiometric proportions and have been subsequently heated to 1273 K for 1 hr in order to evaporate CO$_2$. After mechanical homogenization of the oxide powders, they have been transferred to an electric-arc furnace, where they were molten (see Fabian et al. 2001 for an extensive description of this procedure). Mg$_2$TiO$_4$ has been produced without making use of the electric arc (i.e., by heating the precursor powders only).

For the transmission measurements, the synthesized polycrystalline samples have been ground to powders. After sedimentation, the particle size has been checked by means of transmission electron microscopy. A particle size of less than 1 μm could be achieved. The powders were then embedded in KBr matrices for the MIR measurements and in polyethylene for the FIR measurements. It is generally known that powder transmission spectra are subject to the influence of particle shape effects in the sense that the particles can be roughly described as a continuous distribution of ellipsoids. This must be taken into account when comparing the mass absorption coefficients derived for the Mg titanates with the absorption efficiencies calculated from the optical constants of TiO$_2$, Ti$_2$O$_3$, and CaTiO$_3$.

3.1. CaTiO$_3$ (*Perovskite*)

Perovskite is a naturally occurring—both terrestrial and lunar—mineral belonging to the orthorhombic crystal class. There also exists a low-temperature modification of CaTiO$_3$ with monoclinic symmetry. In orthorhombic CaTiO$_3$, the Ti ions occupy the edges of the nearly cubic unit cells, the O ions are located between them (also on the edges of the cubes), and the Ca ions are located in the unit cell centers. Thus, Ca occurs in a twelvefold coordination and Ti in a sixfold coordination (Luger 1992). Given its proximity to cubic symmetry, the high-temperature modification of CaTiO$_3$ is optically nearly isotropic (Tröger 1971).

Perovskite is a minor component of meteoritic calcium aluminium inclusions (CAIs), melilite and spinel being the major ones (Cloutis & Gaffey 1993). Under terrestrial conditions, perovskite can be converted into anatase by weathering (Banfield & Veblen 1992). It is not clear whether this process can also take place in circumstellar environments.

It was already pointed out by Larimer (1967) that in a cooling gas of cosmic composition, perovskite is among the very first condensates. According to Gail & Sedlmayr (1998), CaTiO$_3$ is stable up to even slightly higher temperatures than TiO$_2$ and the Mg titanates discussed below. Ferguson et al. (2001) pointed out that CaTiO$_3$ is the most abundant titanium-bearing condensate in the atmospheres of red giants and that its formation leads to a very significant depletion of the TiO molecule.

We used a pseudocubic natural perovskite crystal for reflectance measurements and calculated optical constants from them by means of a Lorentz oscillator fit with 10 harmonic oscillators. Figure 9 shows unpolarized reflectance spectra measured on two orthogonal crystal faces labeled "a" and "b." The close coincidence between the two $R(\lambda)$ curves is due to the small deviation of the crystal from cubic symmetry, which is also characteristic of other solids with perovskite structure like SrTiO$_3$. The large reflectance of perovskite even in the far-infrared indicates the presence of a strong, broad oscillator centered at 130 μm
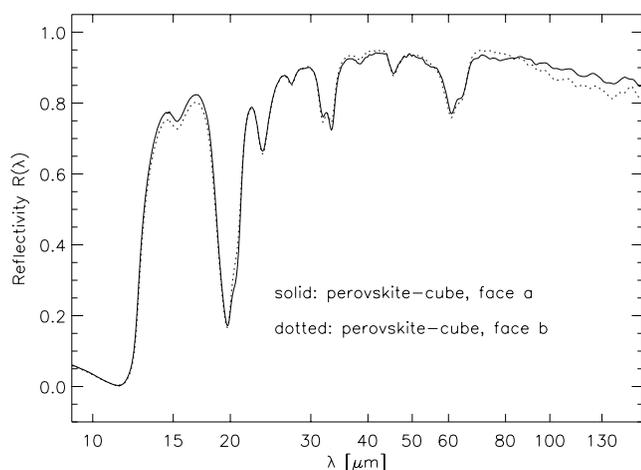
Fig. 9.—Reflectance spectra of perovskite ($CaTiO_3$) measured on two different crystal faces.

Fig. 10.—Emissivity of perovskite ($CaTiO_3$) as derived from its optical constants.

(corresponding to a wavenumber of 75.1 cm^{-1}). This, in turn, leads to very large values of perovskite's optical constants (close to 20 in the 130 μm range). It is evident from the optical constants of the isostructural $SrTiO_3$, published by Palik (1985–1998), that this behavior of n and k is characteristic at least for some titanates with perovskite structure.

Calculations of absorption efficiencies for small spherical particles yield the result that the strongest maximum of perovskite's emissivity is located at 14.1 μm. The corresponding band is very strong and rather narrow (FWHM = 0.8 μm) just as in the case of anatase and Ti_2O_3. Further maxima of C_{abs}/V are located at 21.0, 23.8, 32.7, 33.5, and 62.3 μm (see Figure 10 and Table 2). The 14.1 μm band is most likely to be detected in the spectra of circumstellar shells due to its narrow bandwidth and large intrinsic strength. In ISO-SWS spectra of stars showing the 13 μm feature, a weak bump at 14.1 μm is present, but its reality is contestable due to insufficient signal-to-noise ratios and a sharp drop in the instrument's relative spectral response function between 14.2 and 14.5 μm.

3.2. $MgTiO_3$ (*Geikielite*)

As well as perovskite, geikielite is found on Earth. Its crystal structure is trigonal. It is isostructural to Fe_2TiO_3 (ilmenite), belonging to the space group $R\bar{3}$. Reynard & Guyot (1994) examined the behavior of geikielite at high temperatures and found that (in contrast, e.g., to spinel) no order-disorder transition takes place in the lattice of $MgTiO_3$. Even crystals grown at 1900 K show spectra similar to natural samples.

Based on a factor group analysis, eight infrared active modes of geikieliete (and isostructural titanates like $MnTiO_3$, $NiTiO_3$, etc.) have been predicted (Baran & Botto 1978). For virtually all $MgTiO_3$-like titanates, only six of these eight modes correspond to conspicuous maxima of the absorption efficiency (except for the case of $CoTiO_3$, where all IR active modes can be easily detected in the powder transmission spectra).

We performed powder transmission spectroscopy both on a natural and on synthetic $MgTiO_3$ samples. The natural sample was a piece of gravel from Rakwana, Ceylon. The synthetic sample has been produced under an electric arc

TABLE 2

Overview of the Positions of Spectral Features Produced by Titanium Oxide Particles in the Rayleigh Limit

Substance	Lattice Structure	Band Positions (μm)	FWHM (μm)
Rutile....................	Tetragonal	*13.4*, 23[a], 27.5	1.2
Anatase................	Tetragonal	*13.0*, 15.0, 27.5	0.8
Brookite................	Orthorhombic	*13.5*, 18.5, 21.9, 26.9, 31.1, 33, 44.9, 53.3, 57.5	1.0
Ti_2O_3.....................	Trigonal	*18.6*[b], 20, 25.5, 28, 36	0.8
$CaTiO_3$	Orthorhombic	*14.1*, 21.0, 23.8, 32.7, 33.5, 62.3	0.8
$MgTiO_3$	Trigonal	13.5[c], *17.2*, 21.0, 23.7, 28.0, 35.2	6.9*
$MgTi_2O_5$..............	Orthorhombic	15.4, *19.4*, 24.9[d], 27.7[d], 33.2	6.3*
Mg_2TiO_4..............	Cubic	*16.2*, 20.9, 22.7, 27.4, 35.2	6.2*

Notes.—The respective strongest bands are indicated by italics; the column "FWHM" refers to the width of these strongest bands. Note that FWHM values which have been derived from powder transmission measurements are in general subject to the influence of particle shape effects. Therefore, they are marked with an asterisk (*).

[a] Only present if $T < 1000$ K.
[b] $C_{abs, max}/V < 1\,\mu m^{-1}$.
[c] Shoulder only.
[d] Very weak bands.
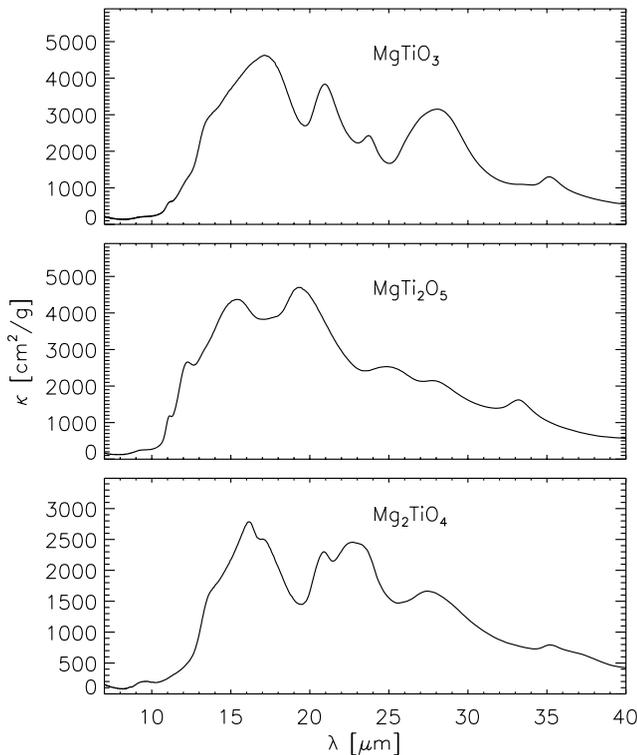
FIG. 11.—Mass absorption coefficients of three synthetic magnesium titanate powder species.

(see above). The natural and the synthetic samples had almost identical spectra. In Figure 11, only the spectrum of the synthetic powder is shown due to the higher purity of the latter.

3.3. $MgTi_2O_5$ (Karrooite)

Karrooite is isostructural to the mineral armalcolite (Mg, Fe)Ti_2O_5, which was first found as a component of lunar rocks. Its stability limit in the (p, T)-plane is very close to that of $MgTiO_3$ and is slightly below the stability limit of $CaTiO_3$ (see Fig. 4 of Gail & Sedlmayr 1998). Ferguson et al. (2001) expect that $MgTi_2O_5$ is among the most abundant Ti-bearing condensates in the atmospheres of M giants.

The strongest opacity maximum of $MgTi_2O_5$ is located at 19.4 μm. Around this wavelength, some oxygen-rich AGB-stars with low mass-loss rates do indeed show a broad emission band (see Posch et al. 2002). Its carrier is most probably some form of magnesiowustite [(Mg, Fe)O]. In principle, $MgTi_2O_5$ is an alternative carrier of the 19.5 μm feature, but an argument against such an identification is the lack of evidence for the secondary karrooite features at 15.4 and 33.2 μm.

3.4. Mg_2TiO_4 (Mg-Titanate Spinel)

Magnesiotitanate spinel has—when synthesized at temperatures above 973 K—an inverse spinel structure (Wechsler & von Dreele 1989). It is nearly realized in nature by the Mg_2TiO_4-rich member of the spinel group, which has been called qandilite. The structural formula of Mg_2TiO_4 is Mg[Mg, Ti]O_4, which means that a part of the Mg ions occupy the tetrahedral interstices of the cubic lattice of oxygen ions, while the Ti ions and the rest of the Mg ions

occupy the octahedral interstices. At temperatures above 1270 K, Mg_2TiO_4 partially decomposes (at atmospheric pressure) into geikielite and MgO. When cooled down rapidly to temperatures below 937 K, Mg_2TiO_4 tends to form a tetragonal phase (Millard, Peterson, & Hunter 1995). This effect, however, is of little relevance for circumstellar shells, where quenching cannot be expected to take place. Note that qandilite can form solid solutions with $MgAl_2O_4$.

We synthesized magnesiotitanate spinel by heating a mixture of $MgCO_3$ and TiO_2 powders to 1723 K for 6 hr. By X-ray diffractometry, we found the synthesis product to have cubic structure and confirmed its homogeneity. The mass absorption coefficient of Mg_2TiO_4 in the 8–40 μm region is shown—together with those of $MgTiO_3$ and $MgTi_2O_5$—in Figure 11.

4. SUMMARY AND ASTROPHYSICAL IMPLICATIONS

Like, for example, SiC (Mutschke et al. 1999), solid titanium dioxide can form various lattice structures belonging to different space groups. The derivation of the optical constants makes it clear that those three TiO_2 modifications which we know as terrestrial minerals do not produce totally different dust emission spectra. More specifically, rutile, anatase, as well as brookite have at least two maxima positions of their absorption cross sections in common. For small spherical particles, these positions are 13–13.5 μm and 26.9–27.5 μm. From (near-spherical) rutile particles, a third prominent maximum of C_{abs} may arise, namely at 23 μm. However, this maximum vanishes for dust temperatures above 1000 K.

If on the basis of the spectroscopy of circumstellar shells a pattern of 13–13.5 and 27.5 μm features were identified, this would be an indication for the presence of some form of solid TiO_2. Obviously, the identification of a 13 μm feature alone is not sufficient, because this feature probably arises from Al–O vibrations in Mg-Al-spinel (Posch et al. 1999; Fabian et al. 2001). Unfortunately, many ISO-SWS spectra are affected by a "red leak" in band 3E (27.4–29.1 μm). In spite of this instrumental problem, Sloan et al. (2003) report the detection of a feature at ~28 μm in sources showing the 13 μm feature. Future observations (e.g., with SIRTF) may help to clarify whether the strength of this feature is indeed correlated with the 13 μm feature strength (which would indicate a common carrier of both bands).

Ti_2O_3, $CaTiO_3$ and Mg-Ti-oxides have their strongest maxima of the absorption coefficient at longer wavelengths than any of the TiO_2 modifications, i.e., in the wavelength range between 14 and 19 μm. The already mentioned Table 2 gives a summary of the crystal structures and band positions of the titanium compounds examined in this paper.

In the present context, it is important to take into account the abundance of titanium compared to that of other metals. According to Palme & Beer (1993), titanium is less abundant than silicon by a factor of about 400 (see also Zimmermann & Schmidt-Burgk 1999). On the other hand, the absorption efficiency of rutile and anatase in the 13 μm region reaches values of up to $C_{abs, max}/V = 5$ μm^{-1}, whereas amorphous (Mg, Fe) SiO_4 is characterized by values of $C_{abs, max}/V \approx 0.11$ μm^{-1} at this wavelength (Dorschner et al. 1995). Hence, TiO_2 particles can radiate about 40 times more efficiently than amorphous silicate particles in the 13 μm region. Together with the abundance ratio, this means that the most prominent TiO_2 emission

band that we predict will be about 1/10th as strong as the silicate dust emission. If the TiO_2 molecules condense more efficiently than SiO molecules, the relative strength of the TiO_2 bands will be correspondingly stronger. For a circumstellar shell *as a whole*, it cannot be expected that all of the available titanium is consumed for the formation of Ti oxides and that, simultaneously, a significantly smaller fraction of the available silicon is bound in amorphous silicates. However, for the *inner part* of circumstellar shells, it was shown, e.g., by Kozasa & Sogawa (1999) that oxides may condense at 3–4 stellar radii where amorphous silicates (due to their larger opacity in the visible and near-IR region) would be heated to a temperature above their condensation temperature. Actually, these authors found the condensation point of corundum (α-Al_2O_3) to be located much closer to the star than the condensation point of silicates; this result is valid for all oxides that are as transparent in the visible and near-IR as α-Al_2O_3, i.e., it is valid for iron-free titanium oxides as well (see Woitke 2000 for a comparison between the equilibrium dust temperatures of these two grain species).

As soon as it is possible to take spatially resolved spectra of the inner parts of circumstellar shells, we will be studying environments in which the conditions figured out above should be fulfilled (very few silicon atoms, but a large fraction of the titanium atoms in the solid phase); therefore, it will be possible to model these spectra with the optical constants of titanium oxides.

REFERENCES

Banfield, J. F., & Veblen, D. R. 1992, Am. Min., 77, 545
Baran, E. J., & Botto, I. L. 1978, Z. Anorg. Allg. Chem., 444, 282
Barshay, S. S., & Lewis, J. S. 1976, ARA&A, 14, 81
Bernatowicz, T. J., et al. 1996, ApJ, 472, 760
Bohren, C. F., & Huffman, D. R. 1983, Absorption and Scattering of Light by Small Particles (New York: Wiley)
Brearley, A. J. 1993, Meteoritics, 28, 590
Burrows, A., & Sharp, C. M. 1999, ApJ, 512, 843
Chigai, T., Yamamoto, T., & Kozasa, T. 1999, ApJ, 510, 999
Cloutis, E. A., & Gaffey, M. J. 1993, Icarus, 105, 568
Dorschner, J., Begemann, B., Henning, Th., Jäger, C., & Mutschke, H. 1995, A&A, 300, 503
Ebel, D. S., & Grossman, L. 2000, Geochim. Cosmochim. Acta, 64, 339
El Goresy, A., Chen, M., Dubrovinsky, L., Gillet, Ph., & Graup, G. 2001, Science, 293, 1467
Fabian, D., Posch, Th., Mutschke, H., Kerschbaum, F., & Dorschner, J. 2001, A&A, 373, 1125
Ferguson, J. W., Alexander, D. R., Allard, F., & Hauschildt, P. H. 2001, ApJ, 557, 798
Gail, H.-P., & Sedlmayr, E. 1998, Faraday Discuss., 109, 303
Gervais, F., & Piriou, B. 1974a, Phys. Rev. B, 10, 1642
———. 1974b, J. Phys. C, 7, 2374
Gonzalez, R. J., & Zallen, R. 1997, Phys. Rev. B, 55, 7014
Helling, Ch., Oevermann, M., Lüttke, M., Klein, R., & Sedlmayr, E. 2001, A&A, 376, 194
Holleman, A. F., & Wiberg, E. 1995, Anorganische Chemie (Berlin: de Gruyter)
Hony, S., Tielens, A. G. G. M., Waters, L. B. F. M., & de Koter, A. 2003, A&A, 402, 211
Jeong, K. S., Chang, Ch., Sedlmayr, E., & Sülzle, D. 2000, J. Phys. B, 33, 3417
Jeong, K. S., Winters, J. M., LeBertre, T., & Sedlmayr, E. 2003, A&A, 407, 191
Jeong, K. S., Winters, J. M., & Sedlmayr, E. 1999, in IAU Symp. 191, Asymptotic Giant Branch Stars, ed. T. Le Bertre, A. Lèbre & C. Waelkens (San Francisco: ASP), 233
Kozasa, T., & Sogawa, H. 1999, in IAU Symp. 191, Asymptotic Giant Branch Stars, ed. T. Le Bertre, A. Lèbre & C. Waelkens (San Francisco: ASP), 239

Larimer, J. W. 1967, Geochim. Cosmochim. Acta, 31, 1215
Linsebigler, A. L., Lu, G., & Yates, J. T., Jr. 1995, Chem. Rev., 95, 735
Lucovsky, G., Sladek, R. J., & Allen, J. W. 1977, Phys. Rev. B, 16, 5452
Luger, P. 1992, in Bergmann-Schaefer, Lehrbuch der Experimentalphysik, vol. 6, ed. W. Raith (Berlin: de Gruyter), 109
Millard, R. L., Peterson, R. C., & Hunter, B. K. 1995, Am. Min., 80, 885
Mutschke, H., Andersen, A. C., Clément, D., Henning, Th., & Peiter, G. 1999, A&A, 345, 187
Nittler, L. R. 2003, Earth Planet. Sci. Lett., 209, 259
Palik, E. D., ed. 1985-1998, Handbook of Optical Constants of Solids, Vols. I–III (Boston: Academic Press)
Palme, H., & Beer, H. 1993, in Landolt/Börnstein, New Series, Group VI, Vol. 3, Subvol. A, Astronomy and Astrophysics, Extension and Supplement to Vol. 2, ed. H. H. Voigt (Berlin: Springer), 205
Posch, Th., Kerschbaum, F., Mutschke, H., Dorschner, J., & Jäger, C. 2002, A&A, 393, L7
Posch, Th., et al. 1999, A&A, 352, 609
Reynard, B., & Guyot, F. 1994, Phys. Chem. Min., 21, 441
Ribarsky, M. W. 1985, in Handbook of Optical Constants of Solids, Vol. I, ed. E. D. Palik (Boston: Academic Press), 795
Salpeter, E. E. 1977, ARA&A, 15, 267
Sloan, G. C., Kraemer, C., Goebel, J., & Price, S. 2003, ApJ, 594, 483
Tarte, P. 1963, Silicates Industriels, 28, 345
Tröger, W. E. 1971, Optische Bestimmung der Gesteinsbildenden Minerale, Part 1: Bestimmungstabellen, 4th ed. (Stuttgart: E. Schweizerbart), 18
Ulyanov, A. A. 1998, in Advanced Mineralogy, vol. 3, ed. A. S. Marfunin (Berlin: Springer), 47
Von Helden, G., et al. 2000, Science, 288, 313
Wechsler, B. A., & von Dreele, R. B. 1989, Acta Crystallogr., B45, 542
Woitke, P. 2000, in Astronomy with Radioactivities, ed. R. Diehl, D. Hartmann, (MPE Rep. 274), 163
Won, D.-J., Wang, C.-H., Jang, H.-K., & Choi, D.-J. 2001, Appl. Phys. A, 73, 595
Zimmermann, H., & Schmid-Burgk, J. 1999, in Landolt/Börnstein, New Series, Group VI, Vol. 3, Subvol. C, Astronomy and Astrophysics, Extension and Supplement to Vol. 2, ed. H. H. Voigt (Berlin: Springer), 35